

Cite this: *CrystEngComm*, 2012, **14**, 908[www.rsc.org/crystengcomm](http://www.rsc.org/crystengcomm)

PAPER

# Mapping the supramolecular chemistry of pyrazole-4-sulfonate: layered inorganic–organic networks with Zn<sup>2+</sup>, Cd<sup>2+</sup>, Ag<sup>+</sup>, Na<sup>+</sup> and NH<sub>4</sub><sup>+</sup>, and their use in copper anticorrosion protective films†

Isurika R. Fernando,<sup>a</sup> Sarut Jianrattanasawat,<sup>a</sup> Nikos Daskalakis,<sup>b</sup> Konstantinos D. Demadis<sup>\*b</sup> and Gellert Mezei<sup>\*a</sup>

Received 9th August 2011, Accepted 13th October 2011

DOI: 10.1039/c1ce06027a

Five compounds based on the versatile pyrazole-4-sulfonate anion (4-SO<sub>3</sub>-pzH = L<sup>-</sup>) were synthesized by the reaction of ligand HL with ZnO, CdCO<sub>3</sub>, Ag<sub>2</sub>O, NaOH and NH<sub>3</sub>, respectively. Crystals of Zn(4-SO<sub>3</sub>-pzH)<sub>2</sub>(H<sub>2</sub>O)<sub>2</sub>, Cd(4-SO<sub>3</sub>-pzH)<sub>2</sub>(H<sub>2</sub>O)<sub>2</sub>, Ag(4-SO<sub>3</sub>-pzH), Na(4-SO<sub>3</sub>-pzH)(H<sub>2</sub>O) and NH<sub>4</sub>(4-SO<sub>3</sub>-pzH) were obtained from aqueous solutions upon evaporation, and were characterized by single-crystal X-ray diffraction, IR and NMR spectroscopy, thermogravimetric analysis and copper corrosion inhibition experiments. We found that the non-isomorphous, 3-dimensional inorganic–organic layered solid state structure of these compounds is determined by an intricate interplay between the size, charge and coordination preference of the cation, and an extended lattice of hydrogen bonds and aromatic interactions. Ligand L<sup>-</sup> incorporates a host of different binding capabilities (metal coordination through the pyrazole N-atom and/or the sulfonate O-atom, hydrogen-bonding both as donor and acceptor, π–π and C–H⋯π interactions). Thin films formed by these complexes on copper metal surfaces were studied by optical microscopy, scanning electron microscopy and energy dispersive X-ray spectroscopy. ZnL<sub>2</sub>, CdL<sub>2</sub>, AgL and NH<sub>4</sub>L, in addition to the free ligand HL, were tested as corrosion inhibitors on copper metal surfaces at three different pH values (2, 3 and 4), and the corrosion rates were quantified. Significant corrosion protection was observed with all compounds at pH 4 and 3.

## 1. Introduction

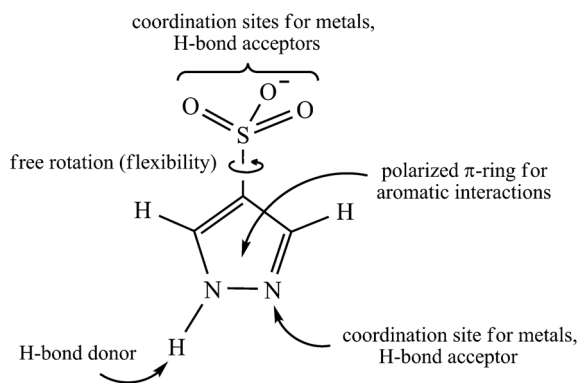
Corrosion of metal surfaces by the environment is a natural process that has significant economic impacts. An extensive study conducted from 1999 to 2001 in 26 industrial sectors in the USA revealed that the approximate direct cost of metallic corrosion is \$276 billion per year, with indirect costs estimated to be equal to the direct costs.<sup>1</sup> Worldwide, the total annual cost of corrosion of \$2.2 trillion is over 3% of the world's gross domestic product (GDP).<sup>2</sup> Copper, although more resistant to reactive environments than other metals used in large-scale industrial and household applications (*i.e.* iron), is susceptible to corrosion especially in the presence of oxygen or other oxidizing agents. Therefore, the development of improved copper corrosion inhibitors is an active field of study.<sup>3</sup> Most importantly, understanding corrosion protection at the molecular level is crucial for the rational design of novel types of inhibitors for customized applications.

Among the various copper corrosion inhibitors studied, heterocyclic aromatic compounds (such as azoles and thiazoles) have been found to be the most effective.<sup>4</sup> N or S donor atoms within these compounds are responsible for the attachment of the inhibitor molecules to the metal surface. In a recent work, we have studied the copper corrosion inhibition efficiency of coordination networks formed by the pyrazole-4-sulfonate anion (4-SO<sub>3</sub>-pzH = L<sup>-</sup>) with various metals, as well as their molecular structure.<sup>5</sup> Single-crystal X-ray crystallographic studies revealed a layered inorganic–organic structure of these materials in which L proves to be an extremely versatile ligand, combining the coordination flexibility of the sulfonate group with the ability of the pyrazole moiety to participate in H-bonding, aromatic interactions and coordination with metals (Scheme 1). Layered inorganic–organic materials have found applications in various fields, such as the fabrication of semiconductor nanocrystals and metal nanoparticles,<sup>6</sup> magnetic materials with tunable properties,<sup>7</sup> multifunctional catalysts,<sup>8</sup> electronics<sup>9</sup> and environmental remediation.<sup>10</sup> Sulfonates, which are structurally similar to phosphonates, have been used as building-blocks for the construction of metal–organic frameworks.<sup>11</sup> In this paper, we report our findings on the effects of Zn, Cd, Ag, Na and NH<sub>4</sub><sup>+</sup> on the structurally adaptable three-dimensional supramolecular frameworks and the copper corrosion inhibition efficiency of these novel materials.

<sup>a</sup>Department of Chemistry, Western Michigan University, Kalamazoo, Michigan, 49008-5413, USA. E-mail: [gellert.mezei@wmich.edu](mailto:gellert.mezei@wmich.edu)

<sup>b</sup>Department of Chemistry, University of Crete, Voutes Campus, Heraklion, Crete, GR-71003, Greece. E-mail: [demadis@chemistry.uoc.gr](mailto:demadis@chemistry.uoc.gr)

† CCDC reference numbers 837807–837811. For crystallographic data in CIF or other electronic format see DOI: 10.1039/c1ce06027a



**Scheme 1** Multiple binding modes of ligand  $L^-$ .

## 2. Experimental section

### 2.1 Materials and methods

All commercially available reagents were used as received. Pyrazole-4-sulfonic acid (HL) was prepared as described previously.<sup>12</sup> Elemental analyses were performed by Galbraith Laboratories, Inc., Knoxville, TN. Infrared, NMR and TGA spectra were recorded on a Bruker Equinox 55 FTIR (in KBr pellets), a Jeol JNM-ECP400 (room temperature) and a Thermal Analyzer TGA Q500 instrument (heated at  $10\text{ }^\circ\text{C min}^{-1}$  from 25 to  $700\text{ }^\circ\text{C}$  under  $\text{N}_2$ ), respectively. SEM/EDS studies were conducted on a scanning electron microscope LEO VP-35 FEM. X-Ray diffraction data were collected at room temperature (298 K) from a single crystal mounted atop a glass fiber with a Siemens SMART 1K CCD diffractometer using graphite-monochromated  $\text{Mo-K}_\alpha$  ( $\lambda = 0.71073\text{ \AA}$ ) radiation. The structures were solved employing the SHELXTL-direct methods program and refined by full-matrix least-squares on  $F^2$ .<sup>13</sup> All non-hydrogen atoms were refined with independent anisotropic displacement parameters. Pyrazole C–H and N–H hydrogen atoms were placed in idealized positions. Water O–H and ammonium N–H hydrogen atoms were located from the difference Fourier map; their displacement parameters were fixed to be 20% larger than those of the attached O or N atoms, and the bond lengths were restrained at 0.82 and 0.89  $\text{\AA}$ , respectively. Crystallographic details are summarized in Table 1.

### 2.2 Synthesis and characterization

Dissolution of HL and  $\text{ZnO}$ ,  $\text{CdCO}_3$ ,  $\text{Ag}_2\text{O}$  or  $\text{NH}_3$ , respectively, in the required molar ratios in  $\text{H}_2\text{O}$  provides the Zn, Cd, Ag and  $\text{NH}_4$ -salts in quantitative yield after removal of the solvent. The Na-salt was obtained using a 2 : 1 molar ratio of NaOH and ligand HL. Colorless crystals suitable for the X-ray diffraction study are obtained by slow evaporation of aqueous solutions. The silver complex was protected from light during its synthesis and crystal growth by covering the reaction/crystallization vessels with aluminium foil, and is stable on long-term storage in the dark.

$\text{ZnL}_2(\text{H}_2\text{O})_2$ : for  $\text{C}_6\text{H}_{10}\text{N}_4\text{O}_8\text{S}_2\text{Zn}$  ( $M_w = 395.71$ ), calculated/found: C, 18.21/18.12%; H, 2.55/2.59%; N, 14.16/13.98%. IR ( $\text{KBr, cm}^{-1}$ ): 3498 s, 3250 s (br), 3131 s, 3017 m, 1640 m, 1543 m, 1496 m, 1396 s, 1231 s (br), 1059 s, 963 s, 883 m, 734 s, 662 s,

572 s, 483 s.  $^1\text{H-NMR}$  (400 MHz,  $\text{D}_2\text{O}$ ): 7.93 ppm (s, 2H).  $\text{CdL}_2(\text{H}_2\text{O})_2$ : for  $\text{C}_6\text{H}_{10}\text{CdN}_4\text{O}_8\text{S}_2$  ( $M_w = 442.71$ ), calculated/found: C, 16.28/16.27%; H, 2.28/2.36%; N, 25.39/25.54%. IR ( $\text{KBr, cm}^{-1}$ ): 3466 s, 3343 s, 3292 s, 3133 s, 1642 m, 1533 s, 1473 s, 1393 s, 1235 s, 1193 s, 1133 s, 1067 s, 959 s, 873 s, 670 s, 591 s.  $\text{AgL}$ : for  $\text{C}_3\text{H}_3\text{AgN}_2\text{O}_3\text{S}$  ( $M_w = 255.00$ ), calculated/found: C, 14.13/14.38%; H, 1.19/1.18%; N, 10.99/10.87%. IR ( $\text{KBr, cm}^{-1}$ ): 3466 s, 3393 s, 3248 s (br), 3161 s, 1689 m, 1644 m, 1533 m, 1473 m, 1390 m, 1206 s, 1059 s, 959 m, 876 m, 761 w, 666 s, 613 s, 539 s, 485 m.  $^1\text{H-NMR}$  (400 MHz,  $\text{D}_2\text{O}$ ): 7.93 ppm (s, 2H).  $\text{NaL}(\text{H}_2\text{O})$ : for  $\text{C}_3\text{H}_3\text{N}_2\text{NaO}_4\text{S}$  ( $M_w = 188.14$ ), calculated/found: C, 19.15/19.09%; H, 2.68/2.71%; N, 14.89/14.85%. IR ( $\text{KBr, cm}^{-1}$ ): 3557 s, 3378 s, 3199 s (br), 3015 s, 2957 s, 1648 s, 1549 s, 1495 s, 1393 s, 1194 s (br), 1136 s, 1061 s, 972 s, 872 s, 794 s, 665 s, 517 s.  $^1\text{H-NMR}$  (400 MHz,  $\text{D}_2\text{O}$ ): 7.93 ppm (s, 2H).  $\text{NH}_4\text{L}$ : for  $\text{C}_3\text{H}_7\text{N}_3\text{O}_3\text{S}$  ( $M_w = 165.17$ ), calculated/found: C, 21.82/22.05%; H, 4.27/4.19%; N, 25.44/25.38%. IR ( $\text{KBr, cm}^{-1}$ ): 3130 s (br), 1702 m, 1645 m, 1549 m, 1401 s, 1207 s, 1060 s, 958 m, 868 m, 798 m, 669 s, 545 m.  $^1\text{H-NMR}$  (400 MHz,  $\text{D}_2\text{O}$ ): 7.93 ppm (s, 2H).

### 2.3 Corrosion inhibition protocols

A modified protocol based on the National Association of Corrosion Engineers (NACE) Standard TM0169-95 is used.<sup>14</sup> Corrosion specimens (copper metal, grade 99.999%, 1 mm thin foil) are cut into  $2 \times 2\text{ cm}$  squares and prepared according to the well-established protocol mentioned above. Each specimen is immersed in a control aqueous solution (no inhibitor) or in a test solution (0.50 mM in L or metal–L complex) at pH = 2.0, 3.0 or 4.0, respectively, and corrosion progress is monitored by visual inspection for a number of days. The duration of the corrosion experiments is variable. For example, for the experiments at pH 2, the duration was  $\sim 4$  days, at pH 3 it was 14–18 days (depending on the individual experiment), and at pH 4 it was 18–19 days (depending on the individual experiment). Longer experiment times were required for the pH 3 and 4 experiments since copper corrosion becomes slower at higher pH values. Then, the specimens are removed from solution, surface samples are taken for spectroscopic studies and the corrosion products are cleaned off the copper surface by the standard NACE method referenced above in order to determine corrosion rates from mass loss. The experimental error for this technique is  $\pm 5\%$ . The corrosion experiments were repeated and the copper specimens were used for optical microscopy, scanning electron microscopy (SEM) and energy dispersive X-ray spectroscopic (EDS) studies.

## 3. Results and discussion

Reaction of pyrazole-4-sulfonic acid in aqueous solution with  $\text{ZnO}$ ,  $\text{CdCO}_3$ ,  $\text{Ag}_2\text{O}$ , NaOH and  $\text{NH}_3$ , respectively, provides the corresponding metal–sulfonate or ammonium–sulfonate complexes, obtained as colorless crystals after water evaporation. All complexes are soluble in water, dimethylsulfoxide and ethylene glycol, but insoluble in other common organic solvents. The anhydrous complexes are thermally stable up to 225–380  $^\circ\text{C}$ .

**Table 1** Summary of crystallographic data

	ZnL <sub>2</sub> (H <sub>2</sub> O) <sub>2</sub>	CdL <sub>2</sub> (H <sub>2</sub> O) <sub>2</sub>	AgL	NaL(H <sub>2</sub> O)	NH <sub>4</sub> L
Formula	C <sub>6</sub> H <sub>10</sub> N <sub>4</sub> O <sub>8</sub> S <sub>2</sub> Zn	C <sub>6</sub> H <sub>10</sub> CdN <sub>4</sub> O <sub>8</sub> S <sub>2</sub>	C <sub>3</sub> H <sub>3</sub> AgN <sub>2</sub> O <sub>3</sub> S	C <sub>3</sub> H <sub>3</sub> N <sub>2</sub> NaO <sub>4</sub> S	C <sub>3</sub> H <sub>7</sub> N <sub>3</sub> O <sub>3</sub> S
Formula weight	395.67	442.70	255.00	188.14	165.18
Crystal system	Triclinic	Monoclinic	Monoclinic	Monoclinic	Monoclinic
Space group	<i>P</i> 1̄ (no. 2)	<i>P</i> 2 <sub>1</sub> / <i>c</i> (no. 14)	<i>P</i> 2 <sub>1</sub> / <i>c</i> (no. 14)	<i>P</i> 2 <sub>1</sub> / <i>c</i> (no. 14)	<i>P</i> 2 <sub>1</sub> / <i>c</i> (no. 14)
<i>a</i> /Å	7.2109(8)	8.668(1)	7.554(2)	10.364(2)	8.919(2)
<i>b</i> /Å	7.3813(9)	10.192(2)	5.4229(1)	7.133(1)	7.241(1)
<i>c</i> /Å	7.3993(9)	7.512(1)	14.260(3)	10.111(2)	11.226(2)
$\alpha$ /°	61.433(2)	90	90	90	90
$\beta$ /°	66.100(2)	95.644(3)	90.590(4)	115.701(2)	101.787(3)
$\gamma$ /°	71.148(2)	90	90	90	90
<i>V</i> /Å <sup>3</sup>	312.10(6)	660.4(2)	584.0(2)	673.5(2)	709.7(2)
<i>Z</i>	1	2	4	4	4
<i>D</i> <sub>calc</sub> /g cm <sup>-3</sup>	2.105	2.226	2.900	1.855	1.546
$\mu$ /mm <sup>-1</sup>	2.351	2.016	3.743	0.508	0.410
Reflections collected/unique	1348/892	2797/949	2438/830	3045/965	3192/1025
Observed reflections ( <i>I</i> > 2 $\sigma$ ( <i>I</i> ))	878	894	753	880	983
Goodness-of-fit (on <i>F</i> <sup>2</sup> )	1.152	1.071	1.053	1.113	1.097
<i>R</i> ( <i>F</i> ); <i>R</i> <sub>w</sub> ( <i>F</i> ) ( <i>I</i> > 2 $\sigma$ ( <i>I</i> ))	0.0251; 0.0690	0.0195; 0.0508	0.0390; 0.1008	0.0258; 0.0749	0.0293; 0.0802
CCDC reference code	837807	837808	837809	837810	837811

### 3.1 Structure description

**Zn(4-SO<sub>3</sub>-pzH)<sub>2</sub>(H<sub>2</sub>O)<sub>2</sub>.** The Zn<sup>2+</sup> center, which lies on a center of inversion, is 6-coordinate in an octahedral environment by four O-atoms (from two SO<sub>3</sub><sup>-</sup> groups and two H<sub>2</sub>O molecules) and two N-atoms from two pyrazole moieties (Fig. 1 and 2, and Table 2). The inorganic layer (Fig. 3) consists of a rectangular pattern of Zn<sup>2+</sup> ions, each coordinated by two SO<sub>3</sub><sup>-</sup> and two H<sub>2</sub>O molecules (Zn⋯Zn distances: 7.2109(8) and 7.5498(7) Å; Zn–Zn–Zn angles: 94.655(4) and 85.345(4)°). The H<sub>2</sub>O molecules form a H-bond with a sulfonate group from a neighboring unit, and a bifurcated H-bond with two sulfonate groups, one bound to the same Zn<sup>2+</sup> ion and the other from a different neighboring unit (Table 3). Within the organic layer, the pyrazole moieties are organized in infinite  $\pi$ -stacked columns (Fig. 4), with plane-to-plane distances of 3.371(3) and 3.384(3) Å and centroid–centroid distances of 3.502(2) and 3.741(2) Å, respectively. The angle between the pyrazole planes is 0° (crystallographically imposed), and the shortest inter-column centroid⋯centroid distance is 7.5498(7) Å. These columns are similar to the ones found in the structure of Cu(4-SO<sub>3</sub>-pzH)<sub>2</sub>(H<sub>2</sub>O)<sub>2</sub>·4H<sub>2</sub>O,<sup>5</sup> except that they do not form H-bonds with H<sub>2</sub>O molecules. The N–H hydrogen atom forms a H-bond with a sulfonate O-atom (Table 3).

**Cd(4-SO<sub>3</sub>-pzH)<sub>2</sub>(H<sub>2</sub>O)<sub>2</sub>.** Similarly to the Zn(4-SO<sub>3</sub>-pzH)<sub>2</sub>(H<sub>2</sub>O)<sub>2</sub> structure, the Cd<sup>2+</sup> ion lies on an inversion center and is 6-coordinate in an octahedral environment by four O-atoms (from two SO<sub>3</sub><sup>-</sup> groups and two H<sub>2</sub>O molecules) and two N-atoms from two pyrazole moieties (Fig. 5 and 2, and Table 4). The inorganic layer (Fig. 3) consists of a rectangular pattern of Cd<sup>2+</sup> ions, each coordinated by two SO<sub>3</sub><sup>-</sup> and two H<sub>2</sub>O molecules (Cd⋯Cd distances: 7.512(1) and 8.668(1) Å; Cd–Cd–Cd angles: 84.356(3) and 95.644(3)°). The H<sub>2</sub>O molecules form a H-bond with a sulfonate group from a neighboring unit and a H-bond with a sulfonate group from the next layer (Table 3). Within the organic layer, the pyrazole moieties are organized in infinite  $\pi$ -stacked columns (Fig. 4), with centroid⋯centroid distances of 3.7653(6) Å and an angle between the pyrazole planes of 20.7(2)°. The inter-column centroid⋯centroid distances are 6.890(2) and 6.488(2) Å. Again, these columns are similar to the ones found in the structure of Cu(4-SO<sub>3</sub>-pzH)<sub>2</sub>(H<sub>2</sub>O)<sub>2</sub>·4H<sub>2</sub>O, except that they do not form H-bonds with H<sub>2</sub>O molecules. The N–H hydrogen atoms of the pyrazole moieties form a bifurcated H-bond with two sulfonate groups (Table 3).

**Ag(4-SO<sub>3</sub>-pzH).** There are two crystallographically independent Ag<sup>+</sup> ions lying on centers of inversion. Both are

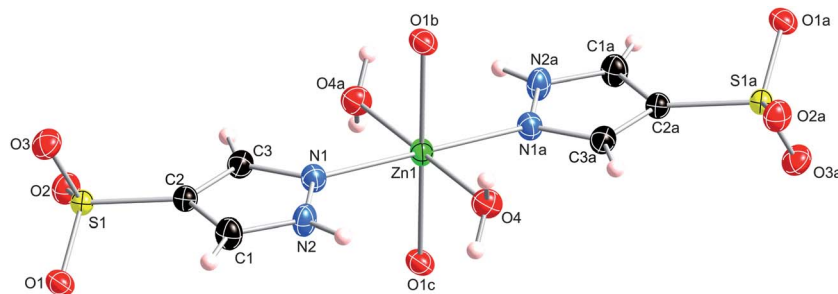


**Fig. 1** Thermal ellipsoid plot (50% probability) of ZnL<sub>2</sub>(H<sub>2</sub>O)<sub>2</sub> showing the coordination sphere around zinc.

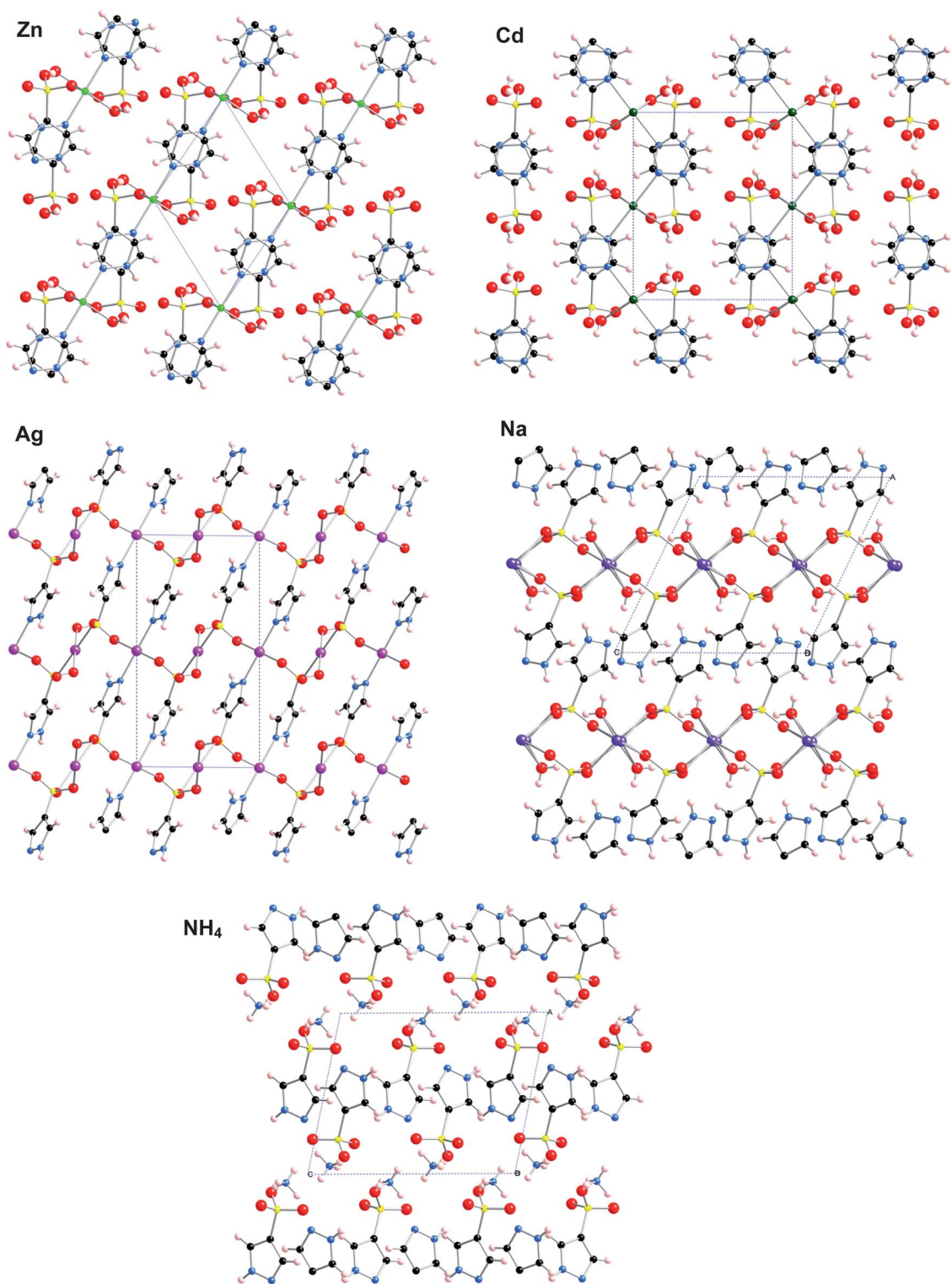


**Fig. 2** View of the alternating inorganic–organic layered structures of  $\text{ZnL}_2(\text{H}_2\text{O})_2$ ,  $\text{CdL}_2(\text{H}_2\text{O})_2$ ,  $\text{AgL}$ ,  $\text{NaL}(\text{H}_2\text{O})$  and  $\text{NH}_4\text{L}$ .

4-coordinate with crystallographically imposed coplanar donor atoms ( $\text{AgO}_4$  and  $\text{AgN}_2\text{O}_2$ ) (Fig. 6 and 2, and Table 5). The inorganic layer (Fig. 3) is built on a rectangular pattern of  $\text{Ag}^+$  ions ( $\text{Ag}\cdots\text{Ag}$  distances: 3.7771(8) and 5.422(1) Å;  $\text{Ag}-\text{Ag}-\text{Ag}$  angles:  $90.00^\circ$ , crystallographically imposed) bound to pyrazole groups and/or  $\mu_3$ -sulfonate groups; it can also be viewed as

chains of  $\text{Ag}^+$  ions ( $\text{AgO}_4$ ) doubly bridged by sulfonate groups and interconnected by the other type of  $\text{Ag}^+$  ions ( $\text{AgN}_2\text{O}_2$ ), which also serve as anchor points for the pyrazole N-atoms. Within the organic layer, the pyrazole moieties are organized into a herringbone pattern by edge-to-face aromatic interactions (Fig. 4), with the closest contacts of  $\text{H}\cdots\text{C}$ : 2.89 Å and 3.11 Å

**Table 2** Selected bond lengths (Å) for ZnL<sub>2</sub>(H<sub>2</sub>O)<sub>2</sub><sup>a</sup>

Zn1–O1b	2.130(2)	S1–O1	1.468(2)
Zn1–O4	2.096(2)	S1–O2	1.455(2)
Zn1–N1	2.141(2)	S1–O3	1.446(2)

<sup>a</sup> Symmetry transformations used to generate equivalent atoms: (a)  $-x, 2 - y, 2 - z$ ; (b)  $x, y, z + 1$ ; (c)  $-x, 2 - y, 1 - z$ .

(H-centroid distances are 2.79 and 3.52 Å; angle between these two vectors: 23.0 and 19.3°, respectively; dihedral angle: 47.6(2)°). The pyrazole N–H hydrogen atom forms a bifurcated H-bond with two O-atoms from different sulfonate groups (Table 3).

**Na(4-SO<sub>3</sub>-pzH)(H<sub>2</sub>O).** The Na<sup>+</sup> ion is 6-coordinate, in a slightly distorted octahedral environment, by six O-atoms from four different SO<sub>3</sub><sup>-</sup> groups and two H<sub>2</sub>O molecules (Fig. 7 and 2 and Table 6). Within the inorganic layer (Fig. 3), the Na<sup>+</sup> ions are found in a distorted rectangular array (within each rectangle, Na···Na distances: 3.5739(5), 4.832(2), 3.5739(5) and 5.287(2) Å; Na–Na–Na angles: 95.86(3), 91.44(3), 88.36(3) and 84.32(3)°). The Na<sup>+</sup> quadrangles are capped by a μ<sub>4</sub>-sulfonate on one side and two μ<sub>2</sub>-H<sub>2</sub>O molecules on the opposite side. Within the organic layer, the pyrazole moieties are organized in a sandwich-herringbone pattern by face-to-face and edge-to-face aromatic interactions (Fig. 4). The distance between the two pyrazole planes (dihedral angle: 0 °C, crystallographically imposed) of the sandwich is 3.25(2) Å, with a centroid···centroid distance of 3.636(2) Å and an angle of 26.6° between these two vectors. The pyrazole sandwiches are further organized in a herringbone pattern by short edge-to-face contacts, H···N: 2.67 Å (H···centroid distance: 2.64 Å; dihedral angle: 83.4(1)°). The pyrazole N–H hydrogen atom forms a H-bond with a sulfonate O-atom, while the N-atom is engaged in a H-bond with the H<sub>2</sub>O molecule. The other H<sub>2</sub>O H-atom forms a H-bond with a sulfonate O-atom (Table 3).

**NH<sub>4</sub>(4-SO<sub>3</sub>-pzH).** Within the inorganic layer, NH<sub>4</sub><sup>+</sup> ions form an undulating sheet with sulfonate groups H-bonded on either side (Fig. 8 and 2, and Table 7). Three of the four ammonium N–H hydrogen atoms form H-bonds with sulfonate groups, while the fourth one is H-bonded to the pyrazole N-atom (Fig. 3). The pyrazole N–H hydrogen atom is also H-bonded to a sulfonate group (Table 3). Within the organic layer, the pyrazole moieties are organized in a sandwich-herringbone pattern by face-to-face and edge-to-face aromatic interactions (Fig. 4). The distance between the two pyrazole planes (dihedral angle: 0 °C, crystallographically imposed) of the sandwich is 3.604(2) Å, with a centroid···centroid distance of 3.752(2) Å and an angle of 16.1° between these two vectors. The pyrazole sandwiches are further organized in a herringbone pattern by edge-to-face interactions, C–H···N: 3.22 Å (H···centroid distance: 3.22 Å; angle between the two vectors: 21.1°, dihedral angle: 66.97(1)°).

### 3.2 Comparison of the molecular and supramolecular structures with other metal-pyrazole-4-sulfonate complexes

Some characteristics of all the pyrazole-4-sulfonate complexes studied so far are compiled in Table 8. Although Zn<sup>2+</sup> has

approximately the same ionic radius as Cu<sup>2+</sup> (0.74 vs. 0.73 Å),<sup>15</sup> the overall solid state structure of the Zn-complex (triclinic, *P* $\bar{1}$ ) is significantly different than the one of the Cu-complex (monoclinic, *P*<sub>2</sub>*1*/*c*): four additional lattice water molecules are found in the case of the Cu-structure. This difference appears to be caused by the slightly different parameters of the otherwise similar coordination spheres of Zn<sup>2+</sup> and Cu<sup>2+</sup> in these two complexes (octahedral with two pyrazole groups, two sulfonate groups and two H<sub>2</sub>O molecules). While all six metal–donor atom distances are within 2.10–2.14 Å in the Zn-complex, the Cu-complex has four shorter (1.97–2.01 Å) and two longer bonds (2.41 Å), a result of Jahn–Teller distortion. The incorporation of the four extra H<sub>2</sub>O molecules *per* complex also leads to a larger separation between the inorganic layers (defined here as the distance between the centers of neighboring inorganic layers) of the Cu-complex (6.65 Å) and the Zn-complex (5.75 Å). Despite these differences, both complexes display an η<sup>1</sup> coordination mode of the sulfonate groups within the inorganic layer (Scheme 2) and stacked pyrazole columns within the organic layer (although water molecules are also included within the organic layer of the Cu-complex).

The larger Cd<sup>2+</sup> ion (0.95 Å) leads to a higher symmetry lattice (monoclinic, *P*<sub>2</sub>*1*/*c*) than the Zn<sup>2+</sup> ion (0.74 Å, triclinic, *P* $\bar{1}$ ), a result of the slightly longer Cd–donor atom bonds (2.28–2.32 Å). Otherwise again, all other structural features are similar (octahedral coordination sphere, η<sup>1</sup> coordination mode of the sulfonate groups and stacked pyrazole columns).

The Ag<sup>+</sup> complex AgL shows the first pyrazole-4-sulfonate structure in which two chemically different Ag<sup>+</sup> centers are found: one (AgN<sub>2</sub>O<sub>2</sub>) has coplanar donor atoms in a distorted square-planar geometry (Ag–N: 2.153(3) Å, Ag–O: 2.803(3) Å, N–Ag–O: 80.0(1) and 100.0(1)°), while the other one (AgO<sub>4</sub>) has a rare, almost perfect square-planar geometry (Ag–O: 2.371(2) and 2.402(2) Å, O–Ag–O: 88.81(8) and 91.19(8)°). Both Ag<sup>+</sup> centers have four additional longer bonds (two on each side) to either N (3.371(3) and 3.377(3) Å for AgO<sub>4</sub>) or O atoms (3.367(3) and 3.440(3) Å for AgN<sub>2</sub>O<sub>2</sub>) making them octacoordinated.

Interestingly, two different Na-complexes were isolated depending on the amount of NaOH added to the aqueous HL solutions. NaL(H<sub>2</sub>O)<sub>2</sub> formed when a 1 : 1 ratio was employed,<sup>16</sup> while NaL(H<sub>2</sub>O) crystallized when we used a 2 : 1 ratio. The symmetry of the NaL(H<sub>2</sub>O) lattice (monoclinic, *P*<sub>2</sub>*1*/*c*) is lower than the one of the NaL(H<sub>2</sub>O)<sub>2</sub> lattice (orthorhombic, *Pbca*). The presence of only one H<sub>2</sub>O molecule *per* NaL unit leads to a coordination sphere containing only two H<sub>2</sub>O molecules around the Na<sup>+</sup> centers (four in the case of NaL(H<sub>2</sub>O)<sub>2</sub>), an increase of the hapticity of the sulfonate group from μ<sub>2</sub>-η<sup>1</sup>:η<sup>1</sup> to μ<sub>4</sub>-η<sup>1</sup>:η<sup>1</sup>:η<sup>2</sup>, a change from herringbone to sandwich-herringbone packing of the pyrazole units within the organic layer and a decrease of the separation between inorganic layers from 10.29 to 9.34 Å.

Although not a metal ion, NH<sub>4</sub><sup>+</sup> behaves practically identical to the similarly sized Cs<sup>+</sup> ion in its complex with the pyrazole-4-sulfonate ligand.<sup>5</sup> For comparison purposes, H-bonds through the N–H hydrogen atoms are considered here as equivalent to coordination bonds. In both anhydrous NH<sub>4</sub><sup>+</sup> and Cs<sup>+</sup> structures the pyrazole moieties within the organic layers are arranged in sandwich-herringbone patterns (Table 8), the sulfonate groups have high hapticity (μ<sub>6</sub>-η<sup>3</sup>:η<sup>2</sup>:η<sup>1</sup> and μ<sub>5</sub>-η<sup>3</sup>:η<sup>2</sup>:η<sup>2</sup>, Scheme 2) and the separation between the inorganic layers is essentially the same (8.73 and 8.82 Å, respectively).

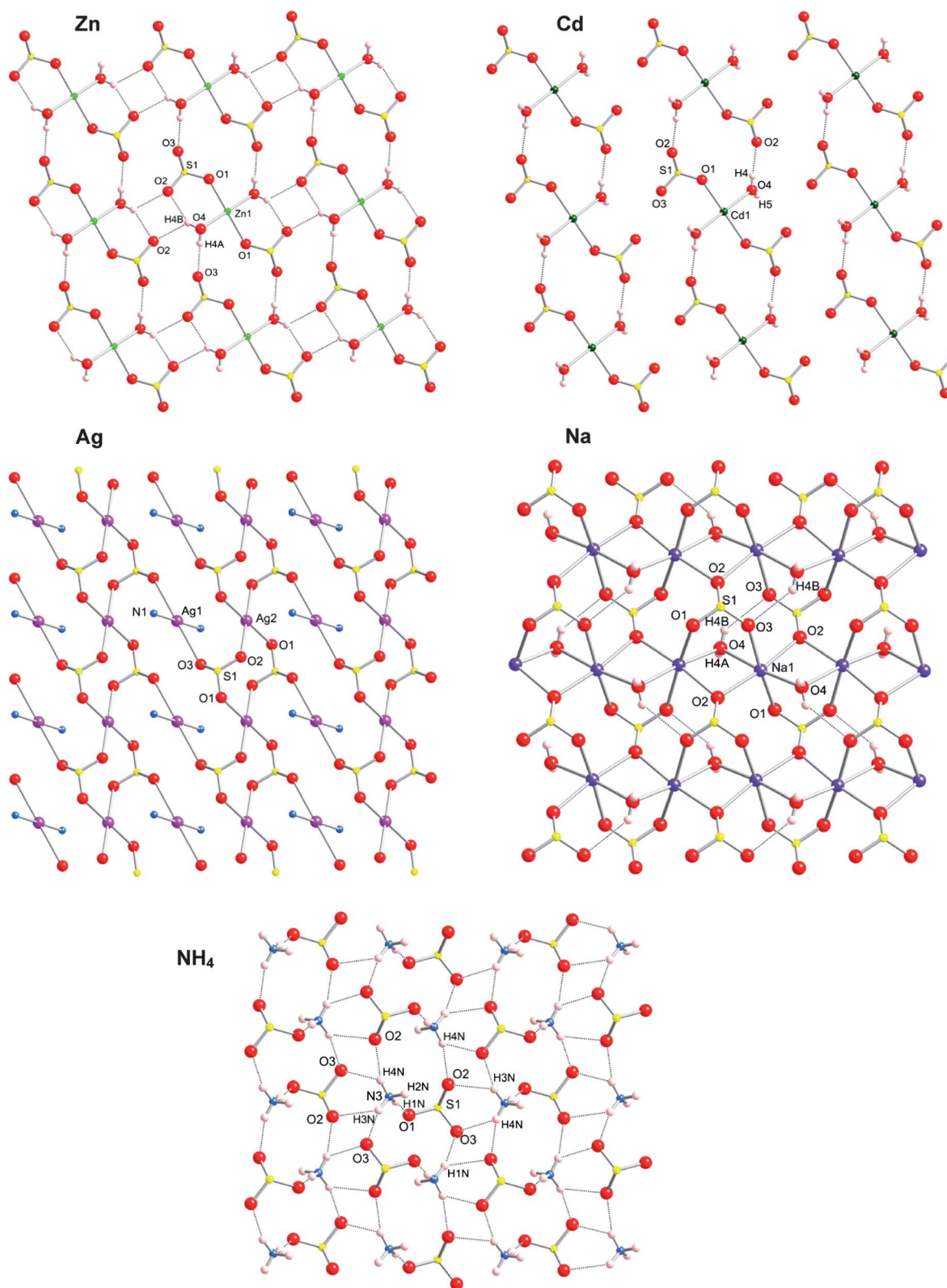


**Fig. 3** Perpendicular view to the inorganic layer in  $\text{ZnL}_2(\text{H}_2\text{O})_2$ ,  $\text{CdL}_2(\text{H}_2\text{O})_2$ ,  $\text{AgL}$ ,  $\text{NaL}(\text{H}_2\text{O})$  and  $\text{NH}_4\text{L}$ .

Besides the structures reported by us here and in two earlier publications, there is only one other reported structure of a metal-pyrazole-4-sulfonate compound:  $[\text{Co}(\text{NH}_3)_5(4\text{-SO}_3\text{-pzH})](\text{ClO}_4)_2 \cdot \text{H}_2\text{O}$ .<sup>17</sup> The crystal lattice of this monomeric

complex does not contain separate inorganic and organic layers, and there are no interactions between the pyrazole moieties (closest pyrazole centroid–centroid distance is 6.26 Å).

**Table 3** Summary of hydrogen bonding data

Compound	D–H...A	D–H/(Å)	H...A/(Å)	D...A/(Å)	D–H...A/°	Symmetry operator for A
ZnL <sub>2</sub> (H <sub>2</sub> O) <sub>2</sub>	O4 H4A O3	0.81(2)	1.91(2)	2.715(3)	174(4)	–x + 1, –y + 2, –z + 2
	O4 H4B O2	0.81(2)	2.26(2)	2.967(3)	147(3)	–x, –y + 2, –z + 2
	O4 H4B O2	0.81(2)	2.41(3)	2.961(3)	126(3)	x, y + 1, z – 1
	N2 H2 O2	0.86	2.06	2.891(3)	161	x, y + 1, z – 1
CdL <sub>2</sub> (H <sub>2</sub> O) <sub>2</sub>	O4 H4 O2	0.81(2)	1.99(2)	2.789(3)	173(4)	–x + 2, –y + 2, –z + 1
	O4 H5 O2	0.80(2)	2.17(2)	2.966(3)	172(4)	–x + 2, y + 0.5, –z + 1.5
	N2 H2 O3	0.86	2.22	2.872(3)	132	x – 1, y, z
	N2 H2 O3	0.86	2.50	3.112(3)	129	–x + 2, –y + 2, –z + 2
AgL	N2 H2 O2	0.86	2.54	3.024(4)	116	–x + 1, y + 0.5, –z + 0.5
	N2 H2 O3	0.86	2.17	2.853(4)	136	x, –y + 0.5, z – 0.5
	O4 H4A N1	0.84(2)	2.12(2)	2.933(3)	163(3)	–x, y + 0.5, –z + 0.5
NaL(H <sub>2</sub> O)	O4 H4B O3	0.81(2)	2.51(2)	3.173(2)	142(3)	x, –y + 0.5, z – 0.5
	N2 H2 O1	0.86	1.99	2.842(2)	172	–x, y – 0.5, –z + 0.5
NH <sub>4</sub> L	N3 H1N O1	0.88(2)	2.01(2)	2.878(3)	176(2)	x + 1, y, z
	N3 H2N N1	0.90(2)	2.05(2)	2.917(3)	161(2)	x, y, z
	N3 H3N O2	0.88(2)	2.50(2)	2.976(3)	115(2)	x + 1, –y + 0.5, z + 0.5
	N3 H3N O3	0.88(2)	2.11(2)	2.945(3)	158(3)	–x + 1, –y, –z + 1
	N3 H4N O2	0.88(2)	2.04(2)	2.869(3)	156(3)	–x + 1, –y + 1, –z + 1
	N3 H4N O3	0.88(2)	2.61(2)	3.125(3)	118(2)	x + 1, –y + 0.5, z + 0.5
	N2 H2 O3	0.86	1.98	2.819(2)	166	–x + 1, y + 0.5, –z + 0.5

### 3.3 Spectral and thermogravimetric analysis

The infrared spectra of the complexes show strong bands in the 1235–1178 cm<sup>–1</sup> region corresponding to vibrations of the sulfonate group.<sup>18</sup> C–H stretching vibrations are observed in the 3132–2956 cm<sup>–1</sup> region. Bands attributed to vibrations of the pyrazole rings spread over the regions 1670–1380 and 1130–530 cm<sup>–1</sup>. The hydrated complexes show broad absorption bands around 3200–3400 cm<sup>–1</sup>, characteristic of the stretching vibrations of N–H and O–H groups involved in extensive H-bonding. The absence of these bands in the spectrum of the Ag<sup>+</sup> and NH<sub>4</sub><sup>+</sup> salts confirms their anhydrous solid state lattice determined by X-ray diffraction.

All five salts show one singlet at 7.93 ppm in their <sup>1</sup>H NMR spectra (in D<sub>2</sub>O) corresponding to the aromatic C–H proton. The invariance of the chemical shift with varying metal ions points to an ionic behavior of these complexes in aqueous solution.

Thermogravimetric analysis (TGA) shows a loss of the two water molecules for ZnL<sub>2</sub>(H<sub>2</sub>O)<sub>2</sub> (calc. 9%, obs. 10%) from 200 to 250 °C. In the case of CdL<sub>2</sub>(H<sub>2</sub>O)<sub>2</sub>, the two water molecules are lost between 200 and 220 °C (calc. 8%, obs. 8%). The water molecule of NaL(H<sub>2</sub>O) is lost between 90 and 110 °C (calc. 10%, obs. 9%). The anhydrous salts (ZnL<sub>2</sub>, CdL<sub>2</sub>, AgL, NH<sub>4</sub>L and NaL) are stable up to 380, 370, 300, 225 and 270 °C, respectively. Decomposition occurs above those temperatures. At 700 °C, the corresponding metal sulfates are left behind in the case of the zinc and sodium salts (58% and 62% loss, respectively), the oxide in the case of the cadmium salt (71% loss), silver metal in the case of the silver salt (58% loss), and complete evaporation is observed in the case of the ammonium salt.

### 3.4 Efficiency of HL and metal–L compounds in copper corrosion inhibition

The corrosion inhibition efficiency of the materials described herein was quantified as the “corrosion rate” (CR), by using the equation:

$$\text{CR} = 87.6 \frac{(\text{mass loss})}{(\text{area})(\text{time})(\text{metal density})}$$

*Units:* CR in mm per year, mass loss in mg, area in cm<sup>2</sup>, time in hours, metal density = 8.94 g cm<sup>–3</sup> (for Cu).

Based on our present (Fig. 9) and previous studies,<sup>5</sup> HL is not effective in inhibiting copper corrosion at pH 2 (its CR is 0.45 mm per year, the same as the “control”), but it does decrease corrosion significantly at higher pH values. At pH 3, for example, a CR of 0.05 mm per year is measured in the presence of HL, compared to 0.31 mm per year in the absence of HL (“control”). A drop in the CR of the “control” upon increasing the pH from 2 to 3 is also observed, which is not surprising, given that the corrosion rates strongly depend on pH and become lower at increasing pH values.<sup>19</sup> A further drop in the CR of the “control” is observed on going from pH 3 to 4 (0.11 mm per year), while a higher than expected value is measured in the presence of HL (0.08 mm per year at pH 4). The higher value of CR at pH 4 than at pH 3 in the presence of HL is attributed to either the buffer used to raise the pH of the solution to 4 (the pH of a 0.5 mM HL solution is 3.37), or/and a dramatic increase of the concentration of L<sup>–</sup> (17% at pH 3, 67% at pH 4), as shown previously.<sup>5</sup> It is known that CR values can rise in the presence of increased concentrations of anionic inhibitors.<sup>20</sup>

In contrast to HL, the Zn<sup>2+</sup>, Cd<sup>2+</sup>, Ag<sup>+</sup> and NH<sub>4</sub><sup>+</sup> salts offer partial corrosion inhibition at pH 2 (~45% corrosion rate decrease, compared to the “control”), with all CRs being approximately the same (~0.25 mm per year) (Fig. 9). These additives demonstrate substantial corrosion inhibition at pH 3 (CRs in the range of 0.04–0.05 mm per year) and pH 4 (CRs in the range of 0.02–0.04 mm per year), compared to the CR for the “control” (0.31 mm per year at pH 3 and 0.11 mm per year at pH 4). There is no dramatic differentiation in anti-corrosion efficiency among the metal–L additives studied here.

### 3.5 Study of protective films

In each experiment, the copper surfaces were photographed after removal from the corresponding solutions. Images from the experiments at pH 4 are shown in Fig. 10. These images show that all copper surfaces are satisfactorily protected in the

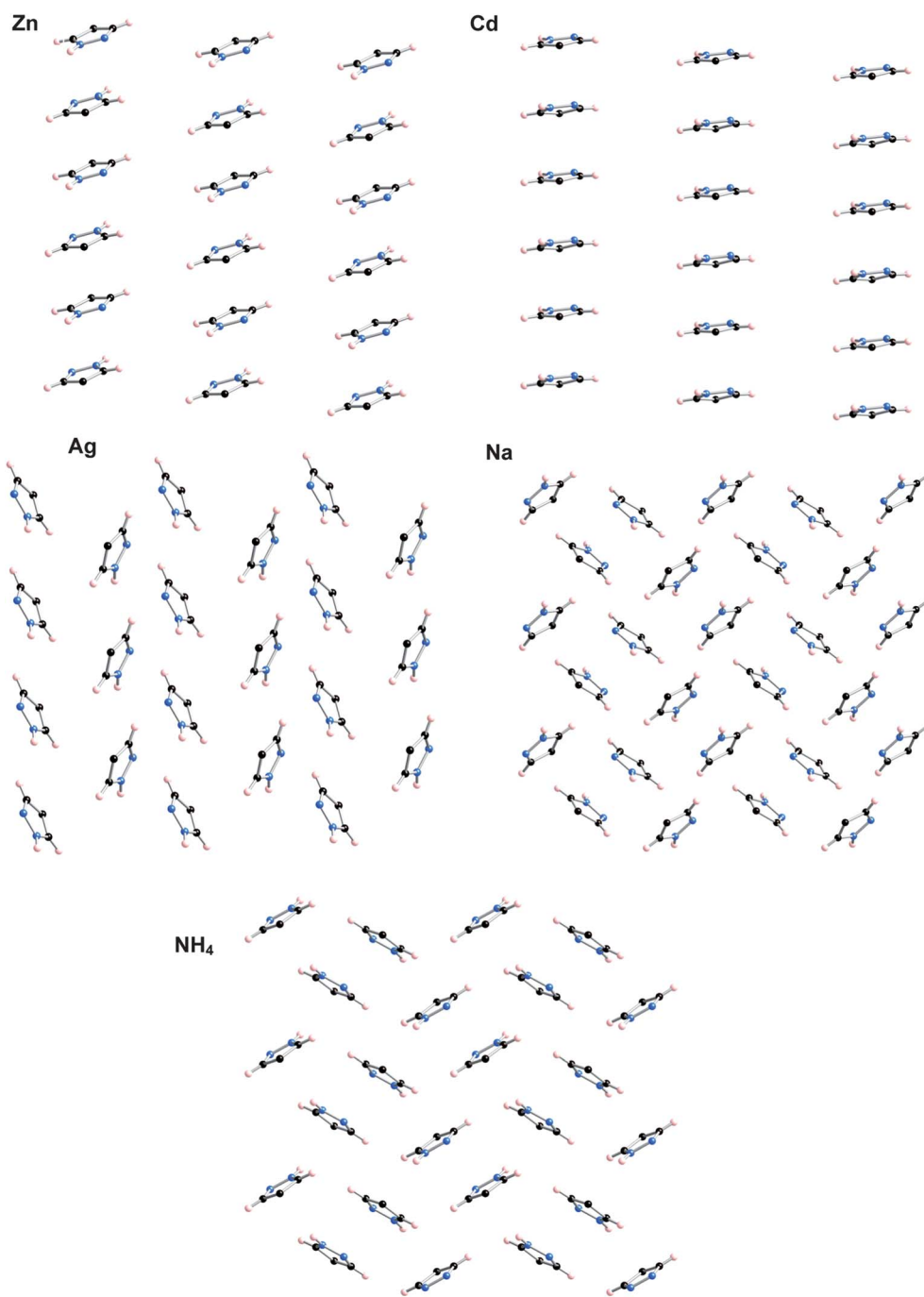


**Fig. 4** Perpendicular view to the organic layer in  $\text{ZnL}_2(\text{H}_2\text{O})_2$ ,  $\text{CdL}_2(\text{H}_2\text{O})_2$ ,  $\text{AgL}$ ,  $\text{NaL}(\text{H}_2\text{O})$  and  $\text{NH}_4\text{L}$ , illustrating the various aromatic interaction patterns.

presence of HL or metal–L complexes. The “control” surface has an obvious layer of green copper-patina. All other surfaces are clean from corrosion products. In some images, slight discolorations can be noted, but they are not the result of ineffective corrosion protection.

Copper specimens were also studied by SEM/EDS. EDS has successfully been used previously in anticorrosion coating composition studies.<sup>21</sup> Fig. 11 shows representative SEM images of the anti-corrosion protective films studied here. The “control”

specimen had a continuous crystalline film of copper oxide (identified by EDS), visible by both optical microphotography and SEM (see image “control”). In the presence of HL (see image “HL”), the surface morphology reveals a much smoother film. The protective films formed by  $\text{ZnL}_2$ ,  $\text{CdL}_2$ ,  $\text{AgL}$  and  $\text{NH}_4\text{L}$  appear very compact, with continuous surface coverage and only some areas showing the presence of pores (see image “ $\text{ZnL}_2$ ”). EDS revealed the presence of the respective cation used in each experiment, thus confirming the formation of metal–L protective

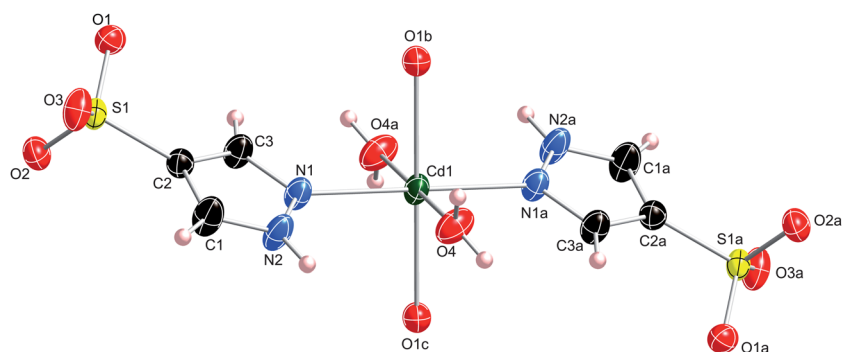


**Fig. 5** Thermal ellipsoid plot (50%) of  $\text{CdL}_2(\text{H}_2\text{O})_2$ , showing the coordination sphere around cadmium.

**Table 4** Selected bond lengths (Å) for  $\text{CdL}_2(\text{H}_2\text{O})_2^a$

Cd1–O1b	2.309(2)	S1–O1	1.463(2)
Cs1–O4	2.320(2)	S1–O2	1.467(2)
Cs1–N1	2.282(2)	S1–O2	1.439(2)

<sup>a</sup> Symmetry transformations used to generate equivalent atoms: (a)  $2 - x, 2 - y, 2 - z$ ; (b)  $2 - x, y + 0.5, 1.5 - z$ ; (c)  $x, 1.5 - y, z + 0.5$ .

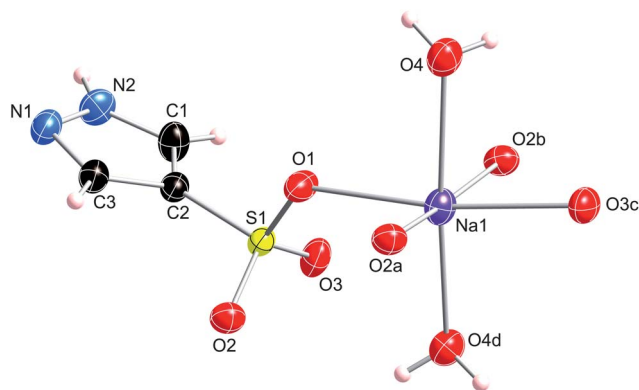
**Table 5** Selected bond lengths (Å) for  $\text{AgL}^a$

Ag1–O3e	2.803(2)	Ag2–O1a	2.371(2)	S1–O1	1.454(3)
Ag1–N1	2.154(3)	Ag2–O2	2.402(2)	S1–O2	1.461(2)
				S1–O3	1.448(3)

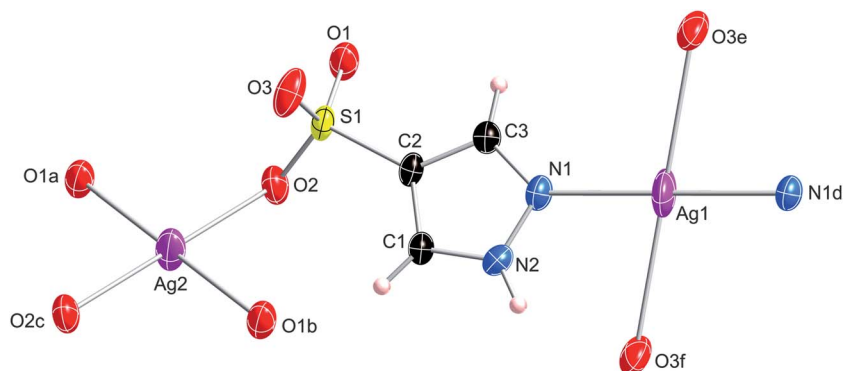
<sup>a</sup> Symmetry transformation used to generate equivalent atoms: (a)  $1 - x, -y, 1 - z$ ; (b)  $x, y + 1, z$ ; (c)  $1 - x, 1 - y, 1 - z$ ; (d)  $-x, -y, -z$ ; (e)  $-x, y - 0.5, 0.5 - z$ ; (f)  $x, 0.5 - y, z - 0.5$ .

films. The film obtained from AgL has a rougher surface, composed of particles of size  $\sim 1$  to  $5 \mu\text{m}$ .

A close examination of the corrosion inhibition results shown in Fig. 9 reveals that the CRs measured in the presence of different metal–L compounds are essentially the same, albeit they are all substantially lower than the “control” (at all three pH values). The lack of a pronounced molecular structure–anticorrosion activity relationship could be attributed to the fact that in all these materials the pyrazole-4-sulfonate ligand coordinates to the metal surface in the same way, through nitrogen atoms of the pyrazole moieties. Given the substantial role N-heterocyclic compounds play in metal corrosion inhibition,<sup>4,22</sup> it is reasonable to assume that the immediate vicinity of the protected copper surfaces studied consists of an organic layer containing the pyrazole moieties, and the inorganic layer containing the different metal ions does not directly interact with the copper surface. Therefore, despite the structural idiosyncrasies of each metal–L compound, corrosion inhibition largely depends on the protective film’s microstructure and morphology. If the protective films of metal–L inhibitors are sufficiently compact (as



**Fig. 7** Thermal ellipsoid plot (50%) of  $\text{NaL}(\text{H}_2\text{O})$ , showing the coordination sphere around sodium.

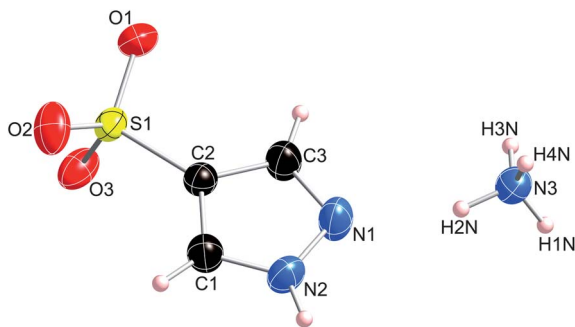


**Fig. 6** Thermal ellipsoid plot (50%) of AgL, showing the coordination sphere around the two crystallographically independent silver atoms.

**Table 6** Selected bond lengths (Å) for NaL(H<sub>2</sub>O)<sup>a</sup>

Na1–O1	2.410(2)	Na1–O3c	2.388(2)	S1–O1	1.458(2)
Na1–O2a	2.385(2)	Na1–O4	2.542(2)	S1–O2	1.454(2)
Na1–O2b	2.409(2)	Na1–O4d	2.458(2)	S1–O3	1.450(2)

<sup>a</sup> Symmetry transformation used to generate equivalent atoms: (a)  $1 - x, -y, 1 - z$ ; (b)  $x, y + 1, z$ ; (c)  $1 - x, 1 - y, 1 - z$ ; (d)  $-x, -y, -z$ ; (e)  $-x, y - 0.5, 0.5 - z$ ; (f)  $x, 0.5 - y, z - 0.5$ .

**Fig. 8** Thermal ellipsoid plot (50%) of NH<sub>4</sub>L.**Table 7** Selected bond lengths (Å) for NH<sub>4</sub>L

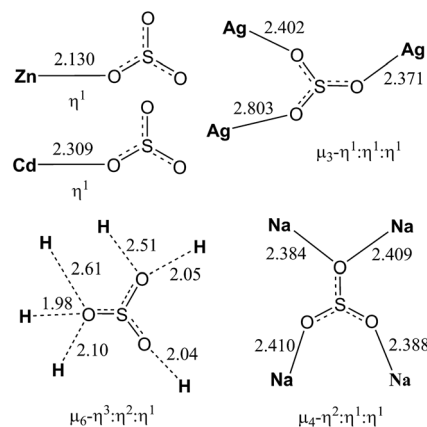
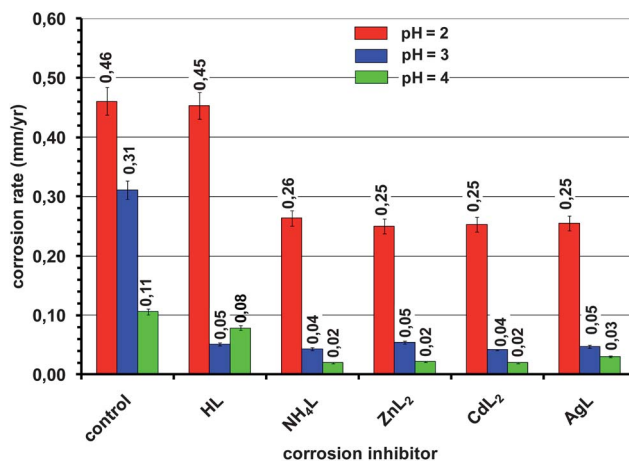
S1–O1	1.444(2)	S1–C2	1.742(2)	N2–C1	1.331(3)
S1–O2	1.440(2)	N1–N2	1.340(3)	C1–C2	1.368(3)
S1–O3	1.459(2)	N1–C3	1.321(3)	C2–C3	1.395(3)

proven by the SEM images in Fig. 11), oxygen diffusion towards the copper surface is minimized, resulting in reduced corrosion rates.

**Table 8** Ionic radii and structural parameters of metal-pyrazole-4-sulfonate complexes

Cation	Ionic radius <sup>a</sup> /Å	Coordi-nation number	Number of coordinated H <sub>2</sub> O molecules	Sulfonate coordination mode	Aromatic interaction pattern	Inorganic layer separation/Å	Ref.
Na <sup>+</sup>	1.02	6	4	$\mu_2\text{-}\eta^1\text{:}\eta^1$	Herringbone	10.29	16
Na <sup>+</sup>	1.02	6	2	$\mu_4\text{-}\eta^1\text{:}\eta^1\text{:}\eta^2$	Sandwich-herringbone	9.34	This work
K <sup>+</sup>	1.51	8	2	$\mu_4\text{-}\eta^2\text{:}\eta^2\text{:}\eta^2$	Sandwich-herringbone	9.96	16
Rb <sup>+</sup>	1.61	8	0	$\mu_4\text{-}\eta^2\text{:}\eta^2\text{:}\eta^2$	Extended T-stacked	6.90	5
Cs <sup>+</sup>	1.78	9	0	$\mu_5\text{-}\eta^3\text{:}\eta^2\text{:}\eta^2$	Sandwich-herringbone	8.82	5
Mg <sup>2+</sup>	0.72	6	6	—	Individual stacks	6.79	5
Ca <sup>2+</sup>	1.06	7	3	$\mu_2\text{-}\eta^1\text{:}\eta^1$ and $\eta^1$	Brickwall	8.96	16
Sr <sup>2+</sup>	1.26	8	0	$\mu_4\text{-}\eta^2\text{:}\eta^1\text{:}\eta^1$ and $\mu_3\text{-}\eta^1\text{:}\eta^1\text{:}\eta^1$	Herringbone	14.17	5
Ba <sup>2+</sup>	1.52	10	1	$\mu_4\text{-}\eta^2\text{:}\eta^2\text{:}\eta^1$ and $\mu_2\text{-}\eta^2\text{:}\eta^1$	Herringbone strips	8.33	16
Cu <sup>2+</sup>	0.73	6	2	$\eta^1$	Stacked columns	6.65	5
Ag <sup>+</sup>	1.28	8	0	$\mu_3\text{-}\eta^1\text{:}\eta^1\text{:}\eta^1$	Herringbone	7.13	This work
Zn <sup>2+</sup>	0.74	6	2	$\eta^1$	Stacked columns	5.75	This work
Cd <sup>2+</sup>	0.95	6	2	$\eta^1$	Stacked columns	5.10	This work
NH <sub>4</sub> <sup>+</sup>	1.75	6	0	$\mu_6\text{-}\eta^3\text{:}\eta^2\text{:}\eta^1$	Sandwich-herringbone	8.73	This work

<sup>a</sup> Effective ionic radii correspond to the observed coordination numbers.<sup>15</sup>

**Scheme 2** Coordination modes (hapticity) of the sulfonate group observed in this work.**Fig. 9** Copper corrosion rates at pH 2, 3 and 4.

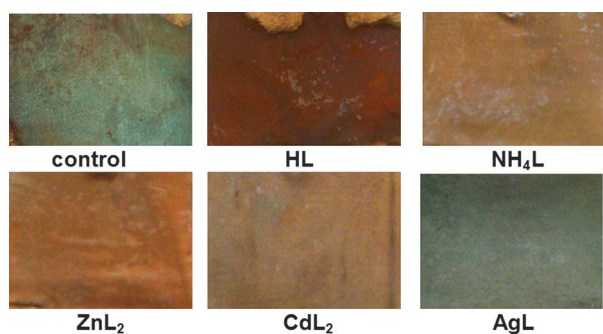


**Fig. 10** Selected images of unprotected (control) and protected surfaces at pH 4. The approximate size of each image is  $1.0 \times 1.5$  cm.

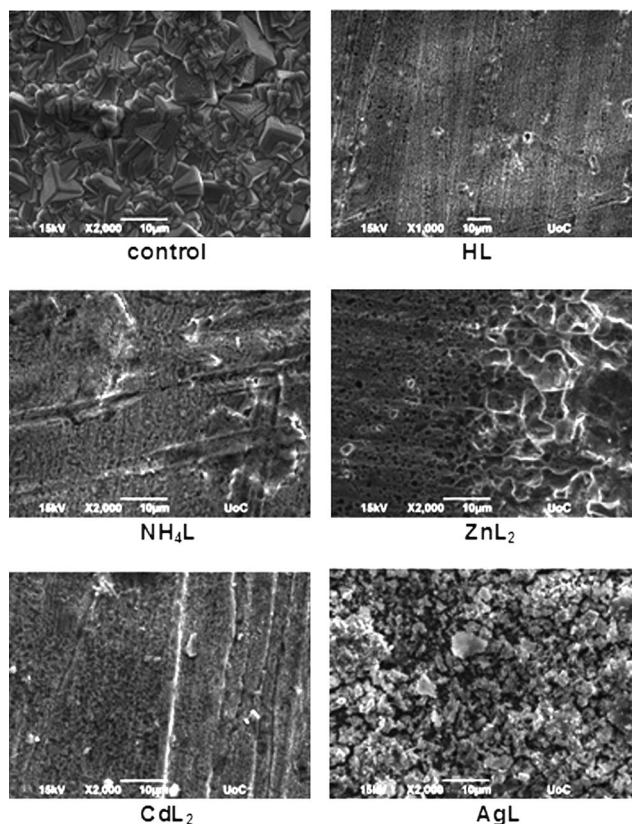


**Fig. 11** SEM images of protective films on copper surfaces at pH 4.

#### 4. Conclusions

As all previously studied pyrazole-4-sulfonate metal complexes,<sup>5,16</sup> the  $Zn^{2+}$ ,  $Cd^{2+}$ ,  $Ag^+$ ,  $Na^+$  and  $NH_4^+$  compounds reported here also display layered inorganic–organic structures in the solid state. In line with previous observations, the larger  $Ag^+$  and  $NH_4^+$  ions form anhydrous complexes, while the smaller  $Zn^{2+}$ ,  $Cd^{2+}$  and  $Na^+$  complexes contain two or one water molecule per “metal–L” unit. Also, a higher hapticity of the sulfonate groups and a more compact packing of the pyrazole groups within the organic layers (herringbone or sandwich-herringbone vs. stacked columns) is observed in the case of the anhydrous complexes. The pyrazole moieties coordinate with the larger ions  $Ag^+$  and  $NH_4^+$  and with the doubly charged metal ions  $Zn^{2+}$  and

$Cd^{2+}$  (also in line with previous observations). In the case of the latter two complexes, we observe the smallest inorganic layer separations of 5.75 and 5.10 Å, respectively. In all cases, the supramolecular structures of these layered materials are the result of the interplay between the coordination preference of the metal ion and the maximization of aromatic interactions and hydrogen bonding, so that all oxygen, nitrogen as well as O–H and N–H hydrogen atoms are involved in an intricate H-bond network. We are currently studying derivatized pyrazole-4-sulfonate complexes of different metals in order to get further insights into their interesting 3-D supramolecular structures, with an emphasis on improved corrosion protection and other potential applications.

#### References

- 1 Federal Highway Administration (FHWA), *Office of the infrastructure and development, report FHWA-RD-01-156: Corrosion cost and preventive strategies in the United States*, 2001.
- 2 G. F. Hays, PE, Director General, *Now is the Time*, World Corrosion Organization, www.corrosion.org.
- 3 (a) M. Finšgar and I. Milošev, *Corros. Sci.*, 2010, **52**, 2737–2749; (b) M. M. Antonijevic and M. B. Petrovic, *Int. J. Electrochem. Sci.*, 2008, **3**, 1–28; (c) J. Mathiyarasu, S. S. Pathak and V. Yegnaraman, *Corros. Rev.*, 2006, **24**, 307–322; (d) Gy. Vastag, E. Szöcs, A. Shaban and E. Kálmán, *Pure Appl. Chem.*, 2001, **73**, 1861–1869; (e) O. M. Magnussen and R. J. Behm, *MRS Bull.*, 1999, **24**, 16–23.
- 4 (a) N. K. Allam, A. A. Nazeer and E. A. Ashour, *J. Appl. Electrochem.*, 2009, **39**, 961–969; (b) M. M. Antonijevic, S. M. Milic and M. B. Petrovic, *Corros. Sci.*, 2009, **51**, 1228–1237; (c) E. Geler and D. S. Azambuja, *Corros. Sci.*, 2000, **42**, 631–643; (d) M. A. Elmorsi and A. M. Hassanein, *Corros. Sci.*, 1999, **41**, 2337–2352; (e) P. G. Cao, J. L. Yao, J. W. Zheng, R. A. Gu and Z. Q. Tian, *Langmuir*, 2002, **18**, 100–104; (f) Y. S. Tan, M. P. Srinivasan, S. O. Pehkonen and S. Y. M. Chooi, *Corros. Sci.*, 2006, **48**, 840–862; (g) S. Ramesh, S. Rajeswari and S. Maruthamuthu, *Appl. Surf. Sci.*, 2004, **229**, 214–225; (h) J.-W. Lee, M.-C. Kang and J. J. Kim, *J. Electrochem. Soc.*, 2005, **152**, C827–C831.
- 5 I. R. Fernando, N. Daskalakis, K. D. Demadis and G. Mezei, *New J. Chem.*, 2010, **34**, 221–235.
- 6 Z. Cheng and J. Lin, *CrystEngComm*, 2010, **12**, 2646–2662.
- 7 P. Rabu and M. Drillon, *Adv. Eng. Mater.*, 2003, **5**, 189–210.
- 8 A. Corma, U. Díaz, T. García, G. Sastre and A. Velty, *J. Am. Chem. Soc.*, 2010, **132**, 15011–15021.
- 9 D. B. Mitzi, K. Chondroudis and C. R. Kagan, *IBM J. Res. Dev.*, 2001, **45**, 29–45.
- 10 A. Mehdi, *J. Mater. Chem.*, 2010, **20**, 9281–9286.
- 11 G. K. H. Shimizu, R. Vaidhyathan and J. M. Taylor, *Chem. Soc. Rev.*, 2009, **38**, 1430–1449.
- 12 C. S. Rondstvedt Jr and P. K. Chang, *J. Am. Chem. Soc.*, 1955, **77**, 6532–6540.
- 13 (a) Data Collection, *SMART-NT Software Reference Manual, Version 5.0*, Bruker AXS, Inc., Madison, WI, 1998; (b) Data Reduction, *SAINT-NT Software Reference Manual, Version 4.0*, Bruker AXS, Inc., Madison, WI, 1996; (c) G. M. Sheldrick, *SHELXTL-NT, Version 5.1*, Bruker AXS, Inc., Madison, WI, 1999.
- 14 NACE Standard TM0169-95 (Item No. 21200), *National Association of Corrosion Engineers*, Houston TX, U.S.A., www.nace.org.
- 15 R. D. Shannon, *Acta Crystallogr., Sect. A: Cryst. Phys., Diffr., Theor. Gen. Crystallogr.*, 1976, **32**, 751–767.
- 16 G. Mezei and R. G. Raptis, *New J. Chem.*, 2003, **27**, 1399–1407.
- 17 H. R. Matthews, L. C. Bucke and A. G. Blackman, *Inorg. Chim. Acta*, 1998, **277**, 89–97.
- 18 R. M. Silverstein, G. C. Bassler and T. C. Morrill, *Spectrometric Identification of Organic Compounds*, John Wiley, New York, 4th edn, 1981, pp. 132–133.
- 19 (a) K. D. Demadis, M. Papadaki, R. G. Raptis and H. Zhao, *Chem. Mater.*, 2008, **20**, 4835–4846; (b) K. D. Demadis, M. Papadaki, R. G. Raptis and H. Zhao, *J. Solid State Chem.*, 2008, **181**, 679–683.

- 
- 20 K. D. Demadis, M. Papadaki and I. Cisarova, *ACS Appl. Mater. Interfaces*, 2010, **2**, 1814–1816.
- 21 (a) K. D. Demadis, P. Lykoudis, R. G. Raptis and G. Mezei, *Cryst. Growth Des.*, 2006, **6**, 1064–1067; (b) K. D. Demadis, C. Mantzaridis and P. Lykoudis, *Ind. Eng. Chem. Res.*, 2006, **45**, 7795–7800; (c) K. D. Demadis, E. Barouda, R. G. Raptis and H. Zhao, *Inorg. Chem.*, 2009, **48**, 819–821; (d) K. D. Demadis, E. Barouda, N. Stavgianoudaki and H. Zhao, *Cryst. Growth Des.*, 2009, **9**, 1250–1253.
- 22 (a) H. Amar, T. Braisaz, D. Villemin and B. Moreau, *Mater. Chem. Phys.*, 2008, **110**, 1–6; (b) J.-J. Fu, S.-N. Li, L.-H. Cao, Y. Wang, L.-H. Yan and L.-D. Lu, *J. Mater. Sci.*, 2010, **45**, 979–986; (c) S. Muralidharan and S. Venkatakrishna Iyer, *Anti-Corros. Methods Mater.*, 1997, **44**, 100–106; (d) A. M. S. Abdennabi, A. I. Abdulhadi and S. Abu-Orabi, *Anti-Corros. Methods Mater.*, 1998, **45**, 103–108; (e) M. Abdallah and M. M. El-Naggar, *Mater. Chem. Phys.*, 2001, **71**, 291–298.